



Research Article

Atorvastatin Entrapped Niosome (Atrosome): Green Preparation Approach for Wound Healing

Shidrokh Abootorabi,¹ Jafar Akbari,^{1,9} Majid Saeedi,^{1,2} Mohammad Seyedabadi,^{3,4} Mohammad Ranaee,^{5,6} Kofi Asare-Addo,⁷ and Ali Nokhodchi^{8,9}

Received 20 December 2021; accepted 4 February 2022; published online 9 March 2022

Abstract. The present study aimed to formulate atorvastatin niosome (Atrosome) through an ultrasonic technique and to determine its contribution to the extent of wound healing in an animal model. The optimized Atrosome formulation (Atrosome-2) was stable at 4 °C for 3 months. Differential scanning calorimetry (DSC), ATR-Fourier transform infrared spectroscopy (ATR-FTIR), and powder X-ray diffraction (PXRD) analysis revealed that atorvastatin (ATR) was well encapsulated within the niosomes either in a stabilized amorphous form or a molecularly dispersed state. Scanning electron microscopy (SEM), transmission electron microscopy (TEM), and atomic force microscope (AFM) confirmed the spherical nature of the Atrosomes. The optimized formulation showed polydispersity index, particle size, drug encapsulation efficiency (EE%), and zeta potential of 0.457 ± 0.05 , 196.33 ± 6.45 nm, 86.15 ± 0.58 %, and -20.73 ± 0.98 mV, respectively. ATR release from the Atrosome gel followed the first-order kinetic model and showed no cytotoxicity in the *in vitro* cytotoxicity test. Cell viability (human foreskin fibroblast cell line) was nearly 99%. An excision wound model was also applied in male Wistar rats to examine the *in vivo* efficacy of the optimized formulation, followed by investigating malondialdehyde (MDA, an end-product of lipid peroxidation), superoxide dismutase (SOD, an endogenous antioxidant), hydroxyproline levels, and glutathione peroxidase (GPx) in skin tissue samples. MDA significantly decreased in the Atrosome gel group after 21 days, while GPx, SOD, and hydroxyproline levels demonstrated an increase. According to histological results, rats receiving Atrosomes were treated effectively faster when compared to the other formulation used.

KEY WORDS: atorvastatin; niosome; wound healing; solid-state analysis; local delivery.

INTRODUCTION

Wound healing is an essentially dynamic and biological procedure that contains four overlapping stages of hemostasis, inflammation, proliferation, and remodeling (1). The above-mentioned stages and their bio-physiological properties should happen in a suitable sequence for restoring the function and form of damaged tissues and cells (2). The regeneration process and wound repair promptly begin following injury through the release of various parameters including fibroblast growth factor 2, cytokines, and vascular endothelial growth factor (3). Oxidative reactions and inflammatory responses also have important contributions to wound healing (4). Some studies report that tissue injury heavily relies on calcium (5), which may have a noticeable contribution to wound healing while affecting the extracellular matrix secretion and F-actin organization in collagen bundles via fibroblasts at the wound area (6). Various modalities have been evaluated by different clinical and experimental studies to treat topical wounds such as antibiotics, sugar, phytotherapy, and honey. Data from human and animal

¹ Department of Pharmaceutics, Faculty of Pharmacy, Mazandaran University of Medical Sciences, Sari, Iran.

² Pharmaceutical Sciences Research Center, Haemoglobinopathy Institute, Mazandaran University of Medical Sciences, Sari, Iran.

³ Department of Toxicology and Pharmacology, Faculty of Pharmacy, Mazandaran University of Medical Sciences, Sari, Iran.

⁴ Pharmaceutical Sciences Research Center7, Faculty of Pharmacy, Mazandaran University of Medical Sciences, Sari, Iran.

⁵ Clinical Research Development Unite of Rouhani Hospital, Babol University of Medical Sciences, Babol, Iran.

⁶ Cancer Research Center, Health Research Institute, Babol University of Medical Sciences, Babol, Iran.

⁷ Department of Pharmacy, University of Huddersfield, Huddersfield, HD1 3DH, UK.

⁸ Pharmaceutics Research Laboratory, School of Life Sciences, University of Sussex, Brighton, BN1 9QJ, UK.

⁹ To whom correspondence should be addressed.
(e-mail: jakbari@mazums.ac.ir; a.nokhodchi@sussex.ac.uk;)

studies reveal that the wound-healing process can be accelerated by statins, particularly ATR (7). Additionally, statins have diverse pleiotropic effects on improving wound healing. The main hurdle when utilizing ATR is that the oral administration is restricted due to its lower aqueous solubility, low bioavailability, and various side effects. Thus, it is critical to discover an alternative administrative route for ATR. The transdermal delivery of ATR is one of the viable and best alternatives since it has numerous advantages (8). Nevertheless, the penetration level into the skin highly relies on the physicochemical characteristics of the chemicals of the vehicle such as the polarity of the solvent, type of vehicle, and particle size (9). With a partition coefficient (logP) of 6.36, a melting point of 176 °C, and a molecular weight of 558.64 g/mol, ATR is an attractive molecule for topical delivery (10). It has been indicated that cosolvents including ethanol and propylene glycol (PG) have improved the solubility of the drugs and thus can be regarded as penetration enhancers. PG can further enter the skin and transmit lipophilic materials via the solvent drag mechanism (9). Based on specific conditions, epidermis penetration via organic chemicals is considered undesirable and must be repressed in conditions where systemic absorption is unnecessary and the side effects of the drug increase due to systemic absorption (11).

Colloidal drug carriers with a surfactant base including niosomes are considered as an operative preparation for transporting higher amounts of drugs through the cutaneous and releasing at a controlled rate during systemic absorption (12). Niosomes are nontoxic and have typically lower production costs and good stability (13). Aghajani et al. have reported niosomes to have beneficial effects in wound healing in an animal model (14). In another study, Farmoudeh et al. found methylene blue-loaded niosome vesicles exhibited a good healing effect on wounds and skin damage (15).

Although there are several studies have assessed niosomal formulation on wound healing (14, 16), none of them has obtained the niosomal formulation via green technology. Therefore, in the current research, the wound healing of the topical gel of Atrosome obtained through a green technology was assessed in rats (no organic solvent involved in the preparation of the formulations). ATR-loaded niosomes were thus developed as a wound-healing agent via the ultrasonic method for local delivery as a substitution to traditional vehicles. Moreover, the effects of the cholesterol ratio were investigated, including the surfactant ratio (w/w) for achieving niosomes with the optimal level of pharmacological response.

MATERIALS AND METHODS

Materials

Atorvastatin calcium (ATR) was purchased from Hakim Pharmaceuticals (Tehran, Iran). Tween 80 and span 80 were obtained from Merck, Germany. Cholesterol was obtained from Solarbio, China.

Preparation of ATR-Niosome (Atrosome)

Ultrasonic processing was used to prepare the ATR loaded niosomes (Atrosome) (17). ATR, cholesterol, span 80, and tween 80 were mixed in a glass vial by magnetic stirring (2,000 rpm) at 70 °C (detail of the composition for each Atrosome

formulation was listed in Table I). The aqueous phase (water), which had been heated on a hot plate and reached 70 °C, was then added to the other components to create a “pre-niosome” using a hot plate magnetic stirrer. Using a probe sonicator, the blend was sonicated with an amplitude of 20% for 3 min (Bandelin, 3100, Germany) followed by submerging the preparation in an ice bath to achieve Atrosome (Table I).

Preparation of Niosomal and ATR Simple Gel

Carbopol 941 (0.75%) gel was obtained by dispersing carbopol in the ATR-niosome (containing 200 mg ATR/20 mL) with preserved water and maintained overnight (12 h). The formulation was then combined and neutralized with dropwise triethanolamine under a propeller homogenizer at 400 rpm to get a suitable gel form. Moreover, ATR (200 mg) was mixed with carbopol 941 dispersion (0.75%) under the propeller homogenizer at 400 rpm to produce the ATR simple gel.

Determination of Particle Size, PDI, and Zeta Potential

Zetasizer Nano ZS system (Malvern Instruments, Worcestershire, UK) was used to determine the particle size, polydispersity index (PDI) and zeta potential of the obtained particles via using the dynamic light scattering (DLS) technique with an angle of 90° at the ambient temperature (25 °C). For each formulation, three separate specimens were obtained, and each sample was repeated three times at room temperature (25 °C) without any dilution (8).

Entrapment Efficiency

The centrifugation technique was used to evaluate the quantity of the encapsulated ATR in the niosomal vesicles. Centrifugation of the niosomal dispersions was performed at 18,000 rpm for 30 min at 4 °C (SIGMA 3-30KS refrigerated centrifuge, Germany) (15). The supernatant layer was filtered (pore size of 0.22 μm) and diluted 100 times, followed by ATR determination in the filtered solution (free drug) using Knauer HPLC. The mobile phase for the HPLC comprised of 30:70 (v/v) combination of water (pH: 3.0 adjusted with 80% phosphoric acid) and methanol. A flow rate of 1.0 mL/min and an XDB-C18 column was used with UV detection at 238 nm. All experiments were conducted at 25 °C. The volume of sample injection and time of sample elution was 20 μL and 30 min, respectively.

Equation 1 was employed to calculate drug entrapment efficiency (EE %) (18).

$$EE\% = \left[\frac{\text{weight of initial drug} - \text{weight of free drug}}{\text{weight of initial drug}} \right] \times 100 \quad (1)$$

Differential Scanning Calorimetry (DSC)

The melting performance of ~ 5 mg of the optimized ATR-niosome particles (Atrosome-2), compared with bulk lipid and parent drug ATR using DSC pyris 6 (PerkinElmer, USA). The particles were sealed into a standard aluminum pan and determined under nitrogen by applying an empty

Table 1 Composition and Properties of Various ATR Niosomes (Atrosome) ($n = 3$, Mean \pm SD)

Formulation	ATR (%w/w)	Cholesterol (%w/w)	Span80 (%w/w)	Tween80 (%w/w)	Water (% w / w)	Particle size (nm)	PDI	ZP (mv)	EE (%)
Atrosome-1	1	0.25	1.25	1.25	96.25	144.7 \pm 13.6	0.45 \pm 0.06	-20.50 \pm 1.15	80.96 \pm 1.65
Atrosome-2	1	0.50	1.25	1.25	96	196.3 \pm 6.5	0.46 \pm 0.05	-20.73 \pm 0.98	86.16 \pm 0.59
Atrosome-3	1	0.75	1.25	1.25	95.75	212.0 \pm 17.5	0.82 \pm 0.06	-19.47 \pm 2.02	86.42 \pm 0.11
Atrosome-4	1	1	1.25	1.25	95.5	236.9 \pm 11.9	0.86 \pm 0.05	-19.30 \pm 1.06	86.51 \pm 0.37
Atrosome-5	1	1.25	1.25	1.25	95.25	351.9 \pm 22.4	0.98 \pm 0.03	-19.100 \pm 0.46	87.18 \pm 0.14

pan as the reference and heated from 30 to 300 °C with a heating rate of 10 °C/min (8).

ATR-FTIR Spectroscopy

The optimized formulation of ATR-niosome (Atrosome-2) was lyophilized for 30 h at -80 °C under 0.1 mbar at -50 °C (Marin Christ, Osterode, Germany). The ATR, freeze-dried Atrosome-2, cholesterol, tween 80, and span 80 were analyzed to determine potential molecular interactions using an ATR-FTIR spectrophotometer (Agilent CARY 630 ATR-FTIR). An average of 32 scans was represented by each ATR-FTIR spectrum at a resolution of 4 cm⁻¹, and the recorded ATR-FTIR spectra were in the range of 4,000–400 cm⁻¹ (19).

Powder X-Ray Diffractometer (PXRD) Analysis

PXRD (Bruker D8, Germany) was employed to study the solid-state of ATR and cholesterol, as well as changes in the solid-state of the lyophilized niosome (Atrosome-2). The instrument was run at 40 kV and 30 mA. The samples were exposed to Cu K α radiation of 1.5406 Å and scanned at a 2 θ of 5–50°, with a step size of 0.040° and a step time of 1 s (8).

Rheological Characterization of Atrosome Gel

The viscosity of the provided ATR niosomal gel was assessed by S-93 spindle on the Brookfield viscometer (DV-II Pro Viscometer, Middleboro, MA), and the viscosity of the sample was measured at different speeds between 0.5 and 100 rpm at (25 \pm 1.0 °C) to measure the subsequent viscosity (20).

In vitro Drug Release

In vitro release evaluation immersion cells, along with acetate cellulose membrane (MWCO 12 kDa), were used for *in vitro* drug-releasing testing (9). Following closing the cells by a cap, the specimens were located in the cells while the acetate cellulose membrane was put on the cells. Then, the cells were placed in the USP dissolution apparatus No. II with each vessel comprising of 900 mL of ethanol: water (50:50). After removing 5 mL of the dissolution medium at different time intervals, the samples were filtered using a 0.22- μ m filter and analyzed using HPLC (refer to entrapment efficiency section). It should be noted that following each sampling time, 5 mL of ethanol: water (50:50) was added to the vessel and the volume of the dissolution medium was maintained.

Kinetic Treatment of the Release Data

The obtained release data from various formulations were fitted to various kinetic models, namely, zero-order, first-order, Higuchi, and Korsmeyer-Peppas models.

$$\text{Zero-order model } M_t = M_0 + K_0 t \quad (2)$$

$$\text{First-order model } \log C = \log C_0 - \frac{K_1 t}{2.303} \quad (3)$$

$$\text{Higuchi model } M_t = k t^{0.5} \quad (4)$$

$$\text{Korsmeyer-Peppas model } \frac{M_t}{M_\infty} = k_p t^n \quad (5)$$

In which, M_0 , M_t , and M_∞ are the amounts of ATR released initially, at time t and at time ∞ , respectively. Further, C_0 and C denote the initial quantities of ATR and at time t , respectively. Likewise, K_0 , K_1 , k , and k_p are considered constants. The value of n was analyzed as the diffusion exponent for investigating the ATR drug release mechanism from each specimen matrices (15).

Scanning Electron Microscopy (SEM)

SEM (FE-SEM TESCAN MIRA3, Czech) was employed to evaluate the morphology of the optimal niosomes (Atrosomes-2). A drop of the sample was placed over a carbon-coated copper grid, and then the sample was air-dried, followed by sputter-coating with gold to make the samples conductive. The images were captured 20 kV accelerating voltage (8).

Atomic Force Microscopy (AFM)

In this experiment, the shape and morphology of the optimal niosomes (Atrosomes-2) were assessed by JPK-AFM (JPK Instruments AG, Berlin, Germany). The samples were diluted 500 times and dropped on the lame and then dried at room temperature (25 °C). Following choosing the contact mode, the photos were taken by repulsive forces (8).

Transmission Electron Microscope (TEM) Analysis

The morphology of Atrosome-2 was examined by a TEM microscope (Philips CM 120 KV, Amsterdam: The Netherlands). A few drops of Atrosome-2 were placed over copper grids coated with carbon. Next, the Atrosome was negatively stained for 30 s by a 2% (v/v) phosphotungstic acid solution. Ultimately, the solvent was evaporated at 25 °C for 24 h before the TEM images were captured (21).

Stability Studies

The stability of the Atrosome-2 was evaluated at 4 and 25 °C for up to three months. Physical stability was monitored, and the effects of temperature and time on the size, ZP, EE%, and PDI, as well as the changes in the color of the formulation and the creation of precipitate aggregation or lipid ingredients were monitored (22).

MTT Assay

Human foreskin fibroblast (HFF) cells were employed *in vitro* (provided by the National Cell Bank, Pasteur Institute of Iran, Tehran, Iran) to analyze the cytotoxicity of the ATR, blank niosome, and Atrosome-2 formulations. The cells were then seeded in the bottom of microplates (Nunclon) for 24 h with the density of 105 cells/wells and 96 wells with Atrosome-2, blank niosome, and ATR (0.5, 1, 1.5, 2, and 2.5 μ M) or the vehicle control. They were then washed with phosphate-buffered saline after the compound removal. Additionally, colorimetry formazan (MTT) was employed to evaluate cell viability. Cell incubation and MTT (0.5 mg/mL) were conducted at 37 °C for 4 h. After discarding the supernatant, the sediment was dissolved in dimethyl sulfoxide (100 μ L) comprising formazan crystals. The plates were agitated for 20 min, and the optical density was

determined using the multi-walled spectrophotometer at 560 nm. Various concentrations (i.e., 0.5, 1, 1.5, 2, and 2.5 μ M) were tested in triplicate with other six controls (the cells in the medium), and finally, the viability of the cells was calculated using Eq. 6:

$$Viability (\%) = \left[\frac{(OD_{sample} - OD_{blank})}{(OD_{control} - OD_{blank})} \right] \times 100 \quad (6)$$

where $OD_{control}$ and OD_{sample} denote the optical density (control) and the optical density (sample) at 560 nm (17), respectively.

Animal Models

Male Wistar rats (200–250 g in weight) were provided from the laboratory animal center of Mazandaran University of Medical Science (MAZUMS), Mazandaran, Iran. The animals were separately kept at a constant temperature (22 °C) and 12 h light/dark cycles and had free access to food and water. The protocol of the study was approved by the Ethics Committee of Mazandaran University of Medical Sciences (the ethical code of IR.MAZUMS.REC.1399.7096).

Full-Thickness Wound Model

Temporary anesthesia was induced by injecting xylazine (20 mg/kg) and ketamine (100 mg/kg) intraperitoneally. After shaving the dorsal hairs, ethanol (70%) was used to clean the skin followed by cutting the skin in a diameter of 2 cm in order to perform full-thickness surgical excisions on the dorsal trunk skin of the rats. The rats were randomly assigned to five groups of nine after the surgery. The animals were classified in group I (Atrosome-2 gel; 1% w/w), group II (ATR simple gel; 1% w/w), and group III (blank niosome gel). In addition, groups IV and V represented the positive control groups receiving phenytoin cream and the negative control group receiving the simple gel respectively. Phenytoin cream was selected as a positive control as it has been used as a wound healing product for many years (23, 24). Furthermore, this product was available on the market as a wound healing product. One gram of gel formulations was topically applied to each group once per day for up to 3 weeks (15).

Monitoring of Wound Healing

The healing procedure was monitored by imaging the lesions at all-time points for all animals using a digital camera after 0, 3, 5, 7, 10, 14, and 21 days. Through digital lesion-area measurements in mm^2 using the software ImageJ (Version 1.45, National Institutes of Health, USA), the lesion areas from the photos were utilized for calculating the wound stoppage using Eq. 7 (25):

$$Wound\ closed (\%) = \left[\frac{Wound\ Area (Day\ X)}{Wound\ Area (Day\ 0)} \right] \times 100 \quad (7)$$

Lipid Peroxidation

For assaying malondialdehyde (MDA) as the end-product of lipid peroxidation in tissue homogenate, a Nalondi

lipid peroxidation (MDA) assay kit (Navand Salamat Company, Urmia, Iran) was utilized, along with the thiobarbituric acid method (26). Briefly, three rats in each group were slaughtered on days 7, 14, and 21. Forty milligram of skin biopsy specimens was obtained at a distance of 2–3 mm thereafter from the wound surrounding area. Next, the tissue specimens were homogenized in butylated hydroxytoluene and lysis buffer, washed with potassium chloride (1.15%), and then cold physiological saline. The debris was removed via centrifuging at 13,000 rpm for 3 min. The combination was heated at 95 °C on a water bath for 45 min after combining 800 µL of 0.67% thiobarbituric acid with 200 µL of tissue homogenate and then cooled in the ice bath for 10 min. The sample absorbance was spectrophotometrically obtained at 550 nm. The obtained UV absorbance data of the specimens were added from the standard curve from the MDA concentrations in the tissue. Finally, lipid peroxidation was normalized based on the amount of the calculated protein from the Bradford assay and the quantity of MDA stated as MDA nanomoles (nM) created per µg of protein.

Glutathione Peroxidase Assay

Tert-butyl-hydroperoxide was used as a substrate to measure GPx activity. Furthermore, NADPH elimination was controlled at 330–350 nm (27). The GPx activity was measured by a Nagpix GPx activity assay kit (Navand Salamat Company, Urmia, Iran). Three rats were sacrificed from each group on days 7, 14, and 21 after which 100 mg of skin biopsy specimens were obtained at a distance of 2–3 mm from the wound margin. The tissue samples were rinsed with potassium chloride (1.15%) and cold physiological saline and then homogenized in assay buffer and finally centrifuged at 9,000 rpm for 15 min at 4 °C to remove the debris. The homogenized samples were made based on kit instructions, and absorption was taken at 340 nm using spectrophotometry. The UV absorption data of the specimens were interpolated from the standard curve for measurements in the tissue. The enzymatic activity was normalized based on the amount of measured protein from the Bradford assay. The activity of glutathione peroxidase in each µg of protein was calculated (one unit of glutathione peroxidase activity is in terms of 1 nmol of the utilized NADPH per minute).

Superoxide Dismutase (SOD) Activity

The total SOD operation of the supernatants was examined in terms of inhibiting the pyrogallol autoxidation based on Marklund (15). A Nasdox SOD activity assay kit (Navand Salamat Company, Urmia, Iran) was applied to determine the SOD activity. The blank and reaction mixtures were made based on the manufacturer's instructions. The enzyme function was measured at 405 nm versus the blank and was determined as per Eq. 8:

$$\text{SOD activity (U/}\mu\text{g pr)} = \left(\frac{OD \text{ Test}}{OD \text{ Blank}} \times 200 \right) / \mu\text{g pr} \quad (8)$$

Finally, enzymatic activity was normalized based on the amount of the calculated protein from the Bradford assay.

Hydroxyproline Test

Hydroxyproline measurements were conducted to determine the value of the density dependence of collagen turnover (28). The hydroxyproline level was calculated by utilizing a hydroxyproline assay kit (Kiazist Company, Hamedan, Iran). Briefly, 40 mg of formulations was homogenized by deionized water. Then, HCl 12 M incubated for 4 h at 120 °C. The sample was then centrifuged at 12,000 rcf for 15 min. A 20 µL of supernatant was taken and followed the kit instructions, and sample absorption was measured at 560 nm using spectrophotometry. Then, the UV absorption data of the specimens were interpolated from the standard curve for measurements in the tissue.

Histology

Three rats were sacrificed from each group on days 7, 14, and 21 after the operation for enzymatic and histopathological examinations. Surgical excision was immediately used and fixed in a 10% formalin solution to remove tissue samples from the wound area. These specimens were then embedded in paraffin blocks to prepare the slices of 4–7 µm. Staining with Masson's trichrome and hematoxylin and eosin was performed after sectioning the samples. Next, the stained sections were observed for any pathological alteration by a light microscope. A scoring system was utilized as a semi-quantitative technique for comparing wound healing between the groups. Seven histological factors were assessed, including granulation tissue thickness, epidermal/dermal regeneration, vascularity, inflammatory cells infiltration, collagen fibers, wound margins distance, and proliferation of fibroblast cells (29). Factors were scored from 0 to 3, and the highest scores were related to the existence of normal structures.

Statistic Evaluation

All data were displayed as the average ± standard deviation and evaluated using SPSS 26.0 (IBM Co., USA). The one-way analysis of variance (ANOVA) and Tukey LSD test were applied for the statistical analysis of the defined variables. Further, one-way ANOVA multiple comparisons and Tukey test LSD's post-hoc test were used for wound healing after the normalization of areas compared to day 0. Furthermore, two-way ANOVA and Tukey LSD post hoc tests were applied for the data assessment of enzymatic tests and hydroxyproline content. Eventually, in the histopathological examination, quantitative data were statistically analyzed by the nonparametric Kruskal-Wallis test (30), and statistical significance was defined as $P < 0.05$ (9).

RESULTS AND DISCUSSION

Properties of Manufactured Niosomes

ATR-loaded niosomes were successfully manufactured using the ultra-sonication technique. Various cholesterol to nonionic surfactant ratios were utilized (a binary mixture of span 80 and tween 80) (1:10, 1:5, 3:10, 2:5, 1:2 w/w) for optimizing the niosomal formulations of ATR. Table 1 presents the niosome compositions and their features. Based on the results, the smallest particle size of niosomes was observed for

Atrosome-1 (144.7 ± 13.6 nm; ratio of cholesterol: surfactant 1:10), and the largest particle size was obtained for Atrosome-5 (351.867 ± 22.414 nm; ratio of cholesterol: surfactants from 1:2). In other words, the vesicle diameter increased by increasing the quantity of cholesterol content from 0.25 to 1.25%. According to Tajbakhsh et al., higher cholesterol contents in niosomes can increase the diameter of niosomes (31).

The percentage of the trapped ATR in the niosome structure varied from 80.96 ± 1.65 to $87.18 \pm 0.14\%$ ($P < 0.0001$, Table I). It is indicated that cholesterol affects the membrane permeation and EE% leading to an alteration in the permeability of the niosomes (32). Likewise, Mokhtar et al. have studied the effect of preparation parameters such as cholesterol content in flurbiprofen niosomes on niosomes properties and have reported that EE% can be optimized by raising the cholesterol, namely, the ratio of surfactants (33).

Table I indicates a slight reduction in the zeta potential of ATR-niosomes when cholesterol is incorporated in the formulation, but this reduction is however not significant ($P > 0.05$). ATR niosomal formulations are favored since they present more stability over mixing and storing with water with the highest zeta potential. This is caused by the electrostatic stabilizing of the formulation (34). The nonionic surfactants interestingly present an unexpectedly negative zeta potential around colloidal particles owing to the dipole nature of the ethoxy groups of nonionic surfactants (35). Radmard et al. assessed the impacts of formulation variables including the cholesterol content of arbutin niosomes and found that zeta potential did not change by increasing the cholesterol content (17).

Generally, the value of the PDI could be within 0–1. The superior formulations with an excellent homogenous dispersion should present values closer to zero (36). As

shown in Table I, the values of the PDI varied between 0.45 ± 0.06 and 0.98 ± 0.03 ($P < 0.0001$). Generally, $PDI > 0.7$ reveals a wide distribution of particle size (8). Based on the findings (Table I), the smallest value of the PDI (0.445 ± 0.056) was related to the formulations possessing 0.25% cholesterol (Atrosome-1), whereas the highest PDI value (0.98 ± 0.03) belonged to the niosome containing the highest cholesterol concentration (Atrosome-5). Additionally, fewer negative charges can be caused by the presence of further cholesterol molecules in niosomes by increasing the agglomeration tendency which leads to higher PDI. This is consistent with the results reported by Radmard et al. (17). Compared with other methods, the present method uses no organic solvent for preparing the niosomes. Moreover, the obtained niosomes can be simply combined with the gel base for obtaining an end-product.

Ideal NPs should possess narrower distribution, lower particle size, high EE%, and high zeta potential. Nonetheless, creating nanoparticles fulfilling all the above-mentioned needs is very challenging. Thus, Atrosome-2 was chosen for further studies since it represented an appropriate percentage of drug entrapment ($86.16 \pm 0.59\%$), the high zeta potential (-20.73 ± 0.98 mV) with a PDI of 0.46 ± 0.05 , and relatively small particle sizes (196.33 ± 6.45 nm).

Differential Scanning Calorimetry

DSC was conducted on the optimized formulation (Atrosome-2), cholesterol, and plain ATR (Figure 1). The DSC traces for cholesterol represented an endothermic sharp peak at 149.26 °C consistent with its melting point

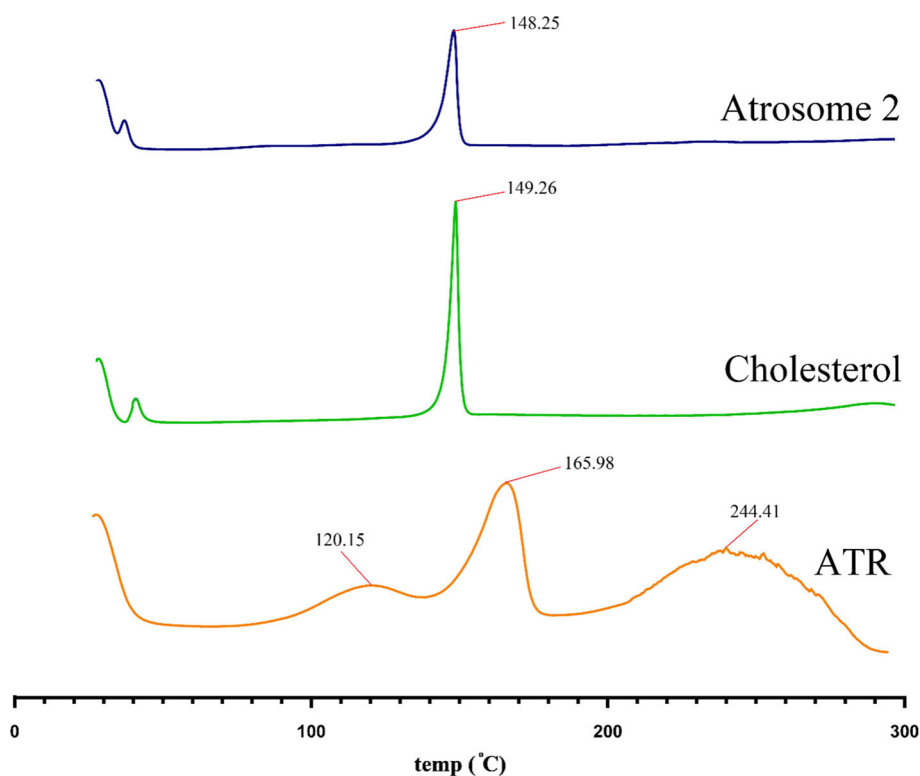


Fig. 1 DSC traces of ATR (atorvastatin), cholesterol, and the optimized Atrosome-2 (atorvastatin-niosome)

(9). DSC traces of plain ATR present three events in the range of 80.87–137.17 °C, 137.17–176.85 °C, and 195.19–289.24 °C. The events are associated with loss of water (80.87–137.17 °C), melting point (165.98 °C), and degradation (195.19–289.24 °C) of the ATR (8). The comparison of the DSC traces of cholesterol and ATR with the DSC traces of Atrosome-2 demonstrated a single endothermic peak near the cholesterol melting peak, while the endothermic peak for the melting of ATR is absent, indicating that ATR in niosome formulations could be in a molecular state. Furthermore, the absence of a diagnostic peak of ATR in the formulation could be the result of the dissolution or miscibility of the ATR in the molten cholesterol. Additionally, the shift in cholesterol peak could be owing to the existence of surfactants (i.e., tween 80 and span 80) in niosome formulations, facilitating the miscibility of cholesterol with the surfactants in niosome.

ATR-FTIR Spectroscopic Studies

The infrared spectra of ATR, cholesterol, tween 80, span 80, and Atrosome-2 are obtained and shown in Figure 2. ATR showed distinctive bands at 3668 cm^{-1} and 3249 cm^{-1} (O–H stretching), 2972 cm^{-1} (N–H stretching), 1649 cm^{-1} (C=O of amide stretching), 1435 cm^{-1} (C–F stretching), 1317 cm^{-1} (C–O stretching), 1215 cm^{-1} (C–N stretching), and 690 cm^{-1} due to aromatic out-of-plane bend (8). Cholesterol represented peaks at 3423 cm^{-1} (O–H stretching), 3000–2850 cm^{-1} (CH– of CH_2 and CH_3 groups and, asymmetric and symmetric stretching), 1465–1457 cm^{-1} (C–H bending), and 1055 cm^{-1} (C–O stretching). tween 80 demonstrated peaks at 3436 cm^{-1} (O–H stretching), 2922 cm^{-1} ($-\text{CH}_2-$ asymmetric stretching), 2858 cm^{-1} ($-\text{CH}_2-$ symmetric stretching), and 1736 cm^{-1} (C=O stretching, ester group), and 1093 cm^{-1} (C–O stretching). Span 80 revealed peaks at 3427 cm^{-1} (O–H stretching), 2925 cm^{-1} (–

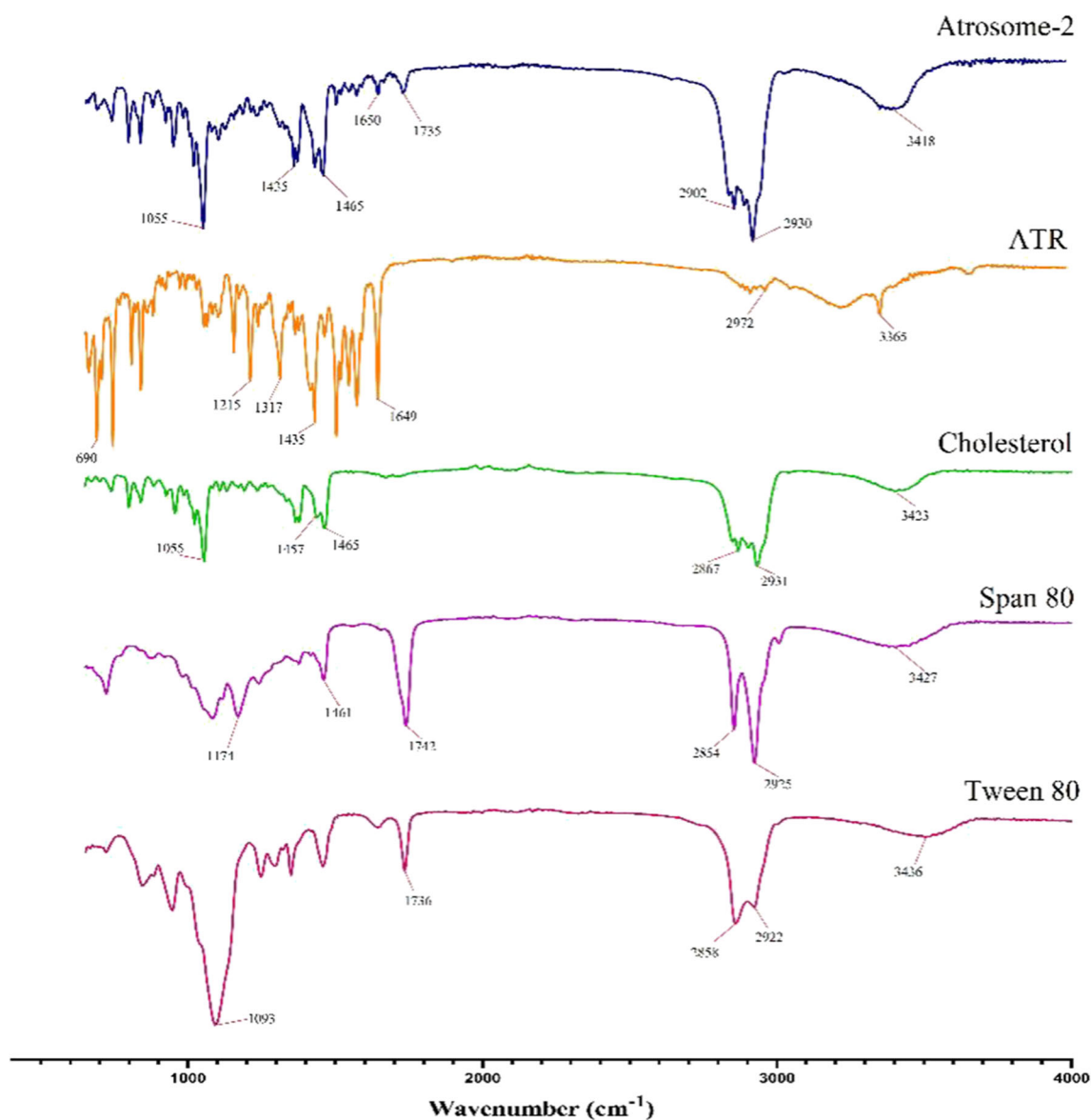


Fig. 2 FT-IR spectra of ATR (atorvastatin), cholesterol, tween 80, span 80, and the optimized Atrosome-2 (atorvastatin-niosome)

CH₂-asymmetric stretching), 2854 cm⁻¹ (-CH₂- symmetric stretching), 1742 cm⁻¹ (C=O stretching), 1680–1600 cm⁻¹ (C=C stretching), 1461 cm⁻¹ (C-H bending), and 1174 cm⁻¹ (C-O bending) (8). FT-IR results proved that there were no chemical interactions between the drug and other components used in the preparation of the niosomes.

Powder X-Ray Diffractometer

The PXRD patterns of ATR, cholesterol, and Atrosome-2 are depicted in Figure 3. ATR revealed several diagnostic peaks at 2θ: 9.50°, 12.40°, 17.50°, 19.55°, 21.70°, 22.80°, and 23.80° (8). The cholesterol represented the peaks at 2θ of 5.30°, 10.60°, 13.15°, 15.55°, 17.05°, 18.20°, 19.45°, 23.55°, 26.20°, 37.15°, and 42.40° (17). These sharp peaks for ATR and cholesterol indicated the highly crystalline nature of the two chemicals. Although cholesterol peaks experienced no shifts in Atrosome-2, it reduced in intensity in comparison with the pure lipid owing to the existence of cholesterol and ATR between the membrane sections of the niosome, thereby altering the cholesterol's crystallinity. The diagnostic peaks for ATR were absent in Atrosome-2 which indicates that ATR is dispersed molecularly or is in an amorphous state within the niosome. This finding is in good agreement with FTIR and DSC analysis.

Rheological Characterization of Atrosome Gel

Rheological attributes of lipid NPs have a deep influence on their capability for topical usage. The Atrosome gel

rheogram is represented in Figure 4, and it shows non-Newtonian flow patterns with no constant viscosity. The flow pattern of Atrosome gels was further recognized by the shear-thinning property with varied thixotropy since the viscosity of the gel decreased by enhancing the rate of the shear. The combined thixotropy and shear thinning performance are ideal properties for topical preparations as the formulation can be taken out of the container by squeezing the container and the formulation becomes high viscose after the application to avoid moving away from the site of application (20).

In vitro Drug Release Study

Figure 5 illustrates the *in vitro* drug release profile of ATR niosomal gel and ATR simple gel. The first-order release model represented the best fit (RSQ = 0.9969) for the niosomal ATR formulation followed closely by Korsmeyer-Peppas (RSQ = 0.9964). In the Korsmeyer-Peppas kinetical model, *n* is the release exponent implying the mechanism of the drug release. The *n* value of the optimized niosomal formulation was in the range of 0.43–0.85, demonstrating that the drug release was based on the non-Fickian (anomalous diffusion) mechanism which includes erosion and diffusion (37). The drug release from vesicles is more likely to occur via the diffusion procedure because of the appropriate data adaptation in the models mentioned above. Figure 5 shows that the drug release from the Atrosome-2 gel formulation (70.91 ± 4.18%) after 24 h was faster than the drug release from the simple ATR gel formulation (48.2 ± 5.59%) (*P* < 0.001).

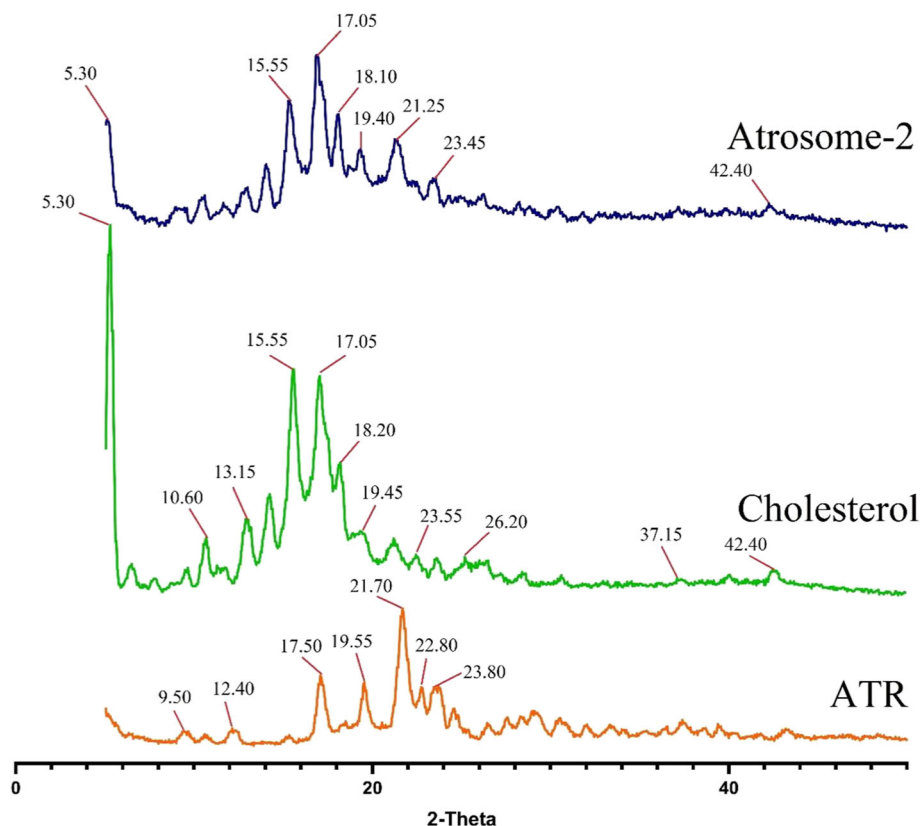


Fig. 3 XRD of ATR (atorvastatin), cholesterol, and the optimized Atrosome-2 (atorvastatin-niosome)

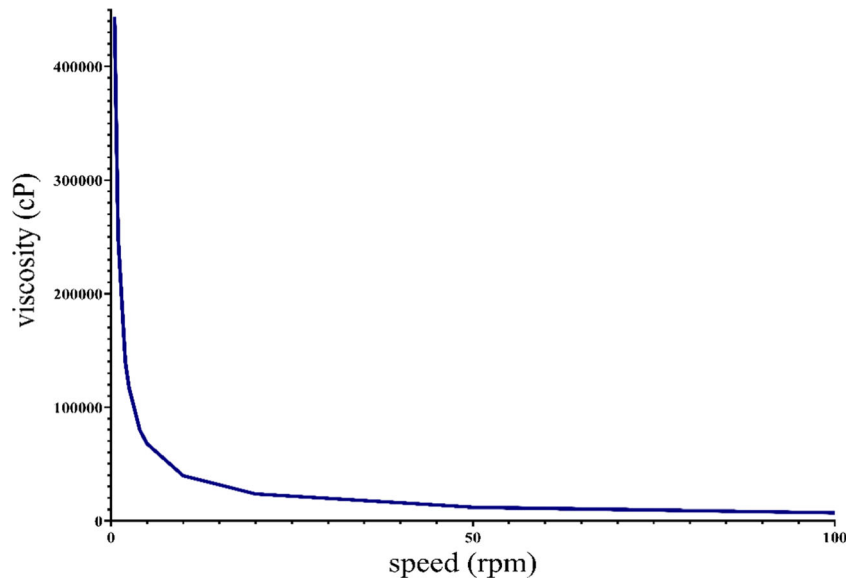


Fig. 4 Viscosity of Atrosome-2 (atorvastatin-niosome) at 25 ± 1 °C

These findings revealed that niosomes can increase the dissolution rate of ATR. Some of the studies are in agreement with the current study; Akbari et al. found that, generally, an increase in the concentration of cholesterol resulted in an increase in the dissolution rate of curcumin from niosome formulations. Niosome formulations with the highest amount of cholesterol showed the fastest dissolution and niosome formulations without cholesterol showed the slowest dissolution. Comparing niosome formulations with the control showed that the incorporation of curcumin in niosome formulation can enhance the dissolution of curcumin (9).

Morphology and Size

The particle size and morphology of NPs were evaluated by SEM, AFM, and TEM. The obtained images for Atrosome-2 (the optimized formulation) by SEM (Figure 6a) and AFM (Figure 6b) revealed that the particles are spherical in shape (SEM image) without any aggregation (AFM image) (8). Based on the TEM images, NPs had nearly uniform spherical shapes with an average size of 180–200 nm (Figure 6c). As shown in the images, there is no aggregation since DLS indicates that the hydrodynamic diameters are based on the intensity and mean particle sizes, whereas TEM

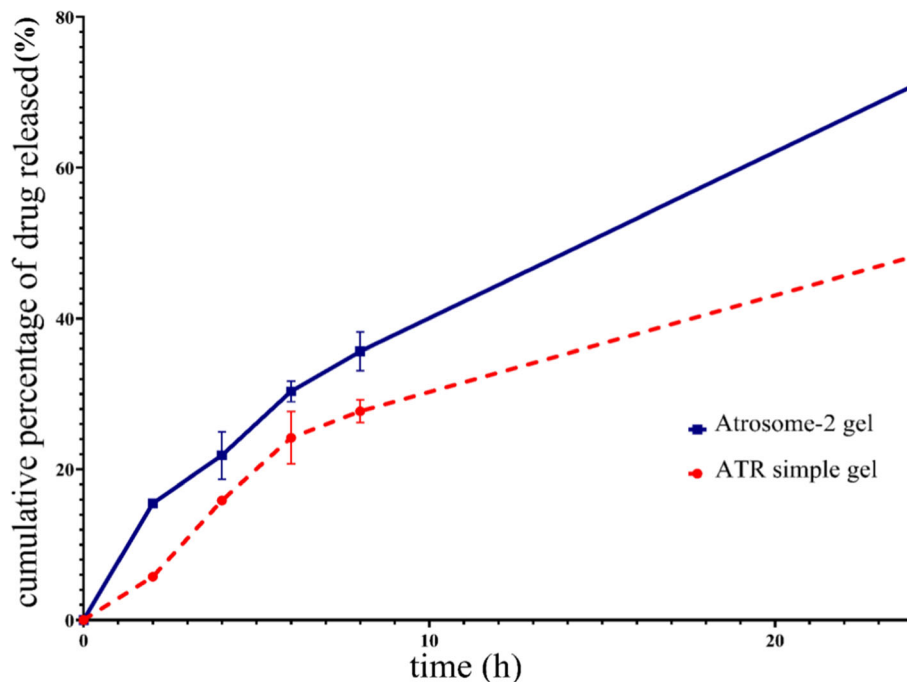


Fig. 5 *In vitro* drug release profile of Atrosome-2, and ATR simple gel

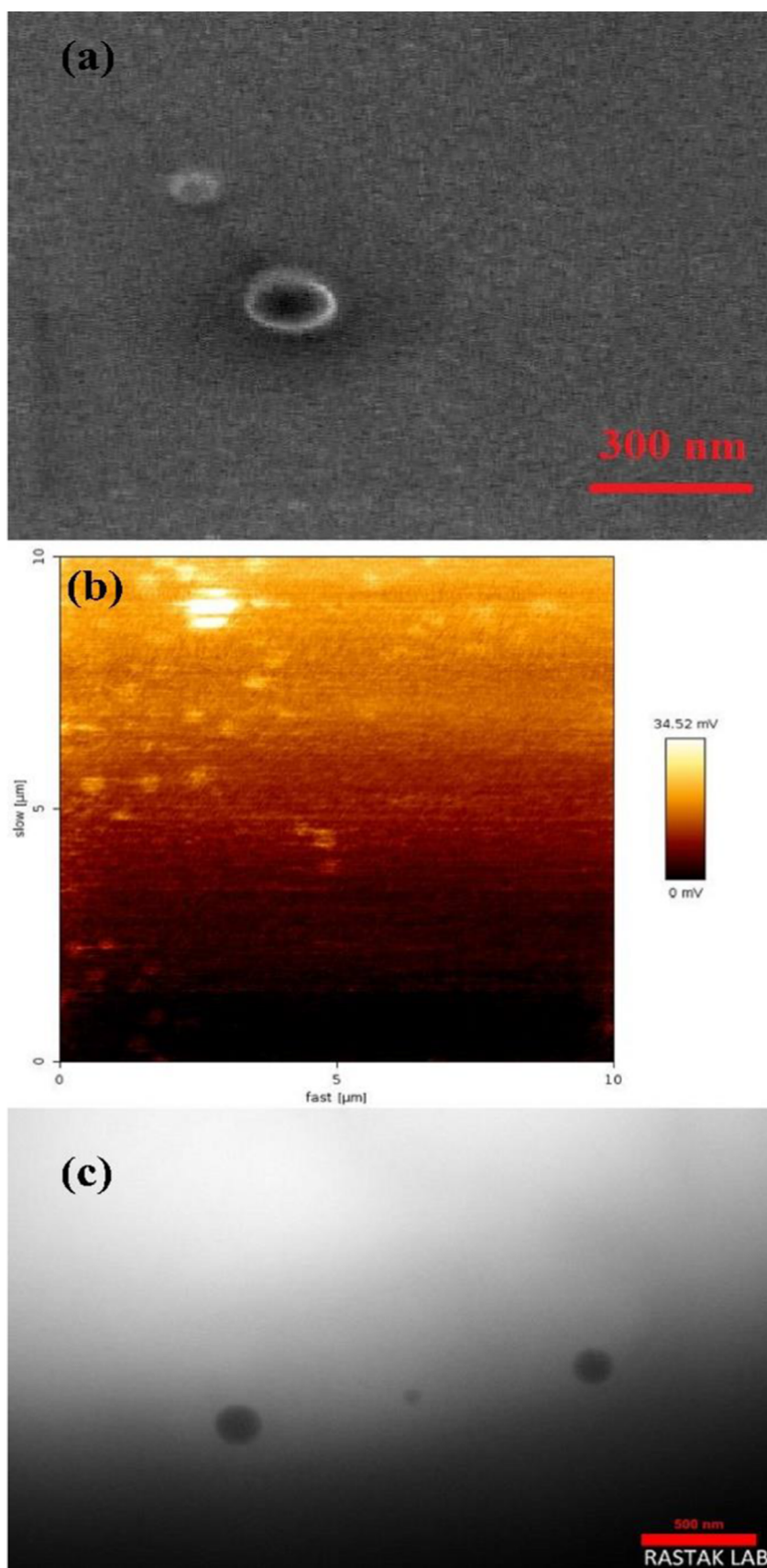


Fig. 6 a SEM, b AFM, c TEM micrographs of Atrosome-2

Table II Stability Information of the Atrosome-2 Dispersion Followed by Storage for 3 months

Storage condition	time	Particle size (nm)	PDI	ZP (mv)	EE (%)
Initial	-	196.3±6.5	0.46±0.05	- 20.73±0.98	86.15±0.58
2-8 °C	3 months	207.5±9.5	0.51±0.04	- 19.11±0.42	84.41±2.72
At room temperature (25 °C)		236.9±15.7	0.67±0.06	- 18.05±0.58	79.02±2.52

acts on dry specimens under ultra-high vacuum circumstances (38). It is noteworthy that the light scattering technique assesses the hydrodynamic radius of the particle, including particle size and related solvent layers. In addition, such dynamic measurement heavily depends on the dispersion behaviors or particle aggregation in the solutions (39).

Stability Studies

Stability was conducted based on zeta potential, entrapment efficiency, particle size, and PDI for three months at 2–8 and 25 °C (Table II). The results indicated that Atrosomes kept at both temperatures were within the same colloidal nanometer range, namely, less than 550 nm (40). Atrosomes kept at 25 °C showed an increment in the PDI (wider distribution as a result of particle growth) and a reduction in EE% and zeta potential. No pronounced alterations were found for Atrosomes kept at 2–8 °C in terms of the properties mentioned above, confirming that 2–8 °C could be a suitable storage temperature for Atrosomes.

In Vitro Cell Viability Study

MTT assay is a test that is based on absorbance and is used for determining the metabolic activity of living cells. To analyze the Atrosome's effects on cell viability, the human foreskin fibroblast cell line was incubated with various concentrations of blank niosome, free ATR, and ATR-trapped niosomes at 0.5–2.5 μM for 24 h (Figure 7). At equal concentrations (0.5–2.5 μM), no noticeable decrease was observed in the vitality of the cells over 24 h when blank niosomes and Atrosomes were used ($P > 0.05$). Based on the obtained data, 98.1 and 99.7% of the cells survived after treatment with blank niosomes and Atrosomes (2.5 μM) for 24 h, respectively. The survival cell in the case of ATR was 79.9%. The findings revealed that ATR had cytotoxicity effects on the HFF normal cell line, while Atrosome presented no cytotoxicity effects, which is in agreement with the results of Çelik et al., who demonstrated an increase in cytotoxicity in human neuroblastoma cell lines (SHSY-5Y) in terms of various ATR concentrations (41). The surface charge of the nanoparticles (NPs) led to greater reactivity with cells

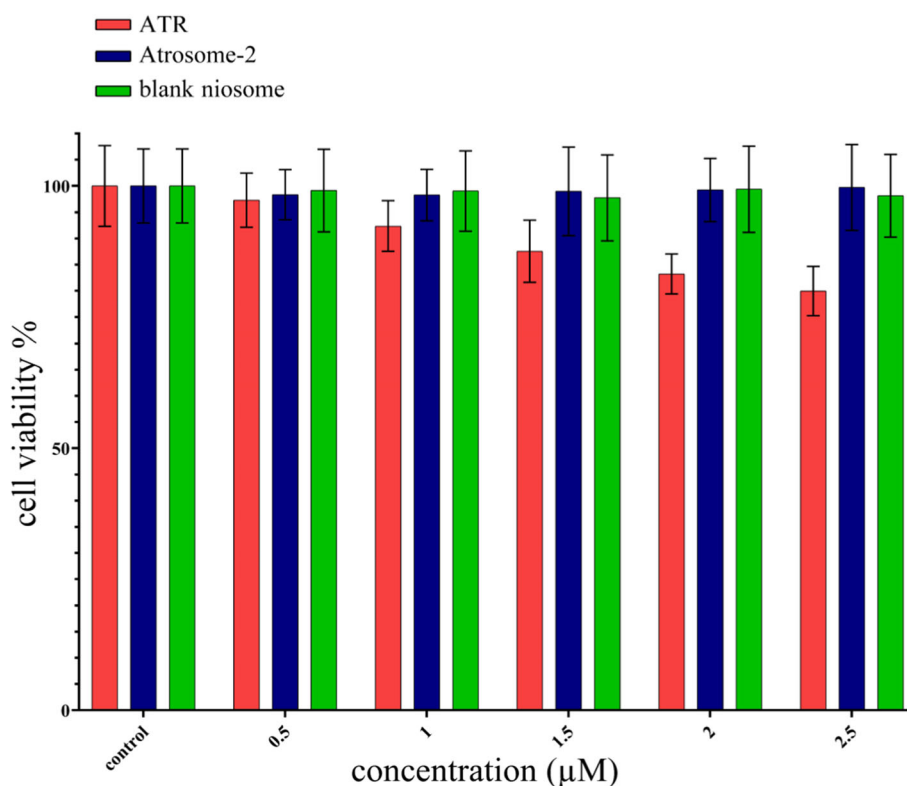


Fig. 7 Viability of cell at various concentrations ATR, blank niosome, and Atrosome -2 (data are mean \pm SD, $n = 8$)

and protein. Nonetheless, the potential values of NPs decreased by loading ATR possibly owing to the uniform distribution of cholesterol and free ATR in the potential diffusion layer or the water phase, resulting in lower toxicity and decreased charge density around the particle (31).

In Vivo Wound Healing Examination

The optimized Atrosome formulation was transformed into the gel base and was topically used for *in vivo* wound healing evaluations. Figure 8a depicts the images generated of the wound area regression over the testing time period. The determined wound area as the primary wound area percentage was defined for all animal groups (Figure 8b).

Based on the obtained data, a significant difference was observed within the subjects across the time in the wound closure ($P < 0.001$). Furthermore, animals receiving different treatments displayed different levels of wound area ($P < 0.001$). Additionally, Atrosome was associated with a more rapid reduction in the wound area in comparison to the ATR simple gel (mean difference: 37.05 mm^2 , $P < 0.001$), blank niosome gel (mean difference: 71.85 mm^2 , $P < 0.001$), and phenytoin cream (mean difference: 45.99 mm^2 , $P > 0.001$). In a previous study performed by Morsy et al. (42), topical treatment with ATR nanoemulgel enhanced tissue recovery in the acute injuries of healthy rats compared with the ATR gel ($P < 0.05$). Based on the histological assessment of the wounds, Adami et al. reported that statin-treated animals

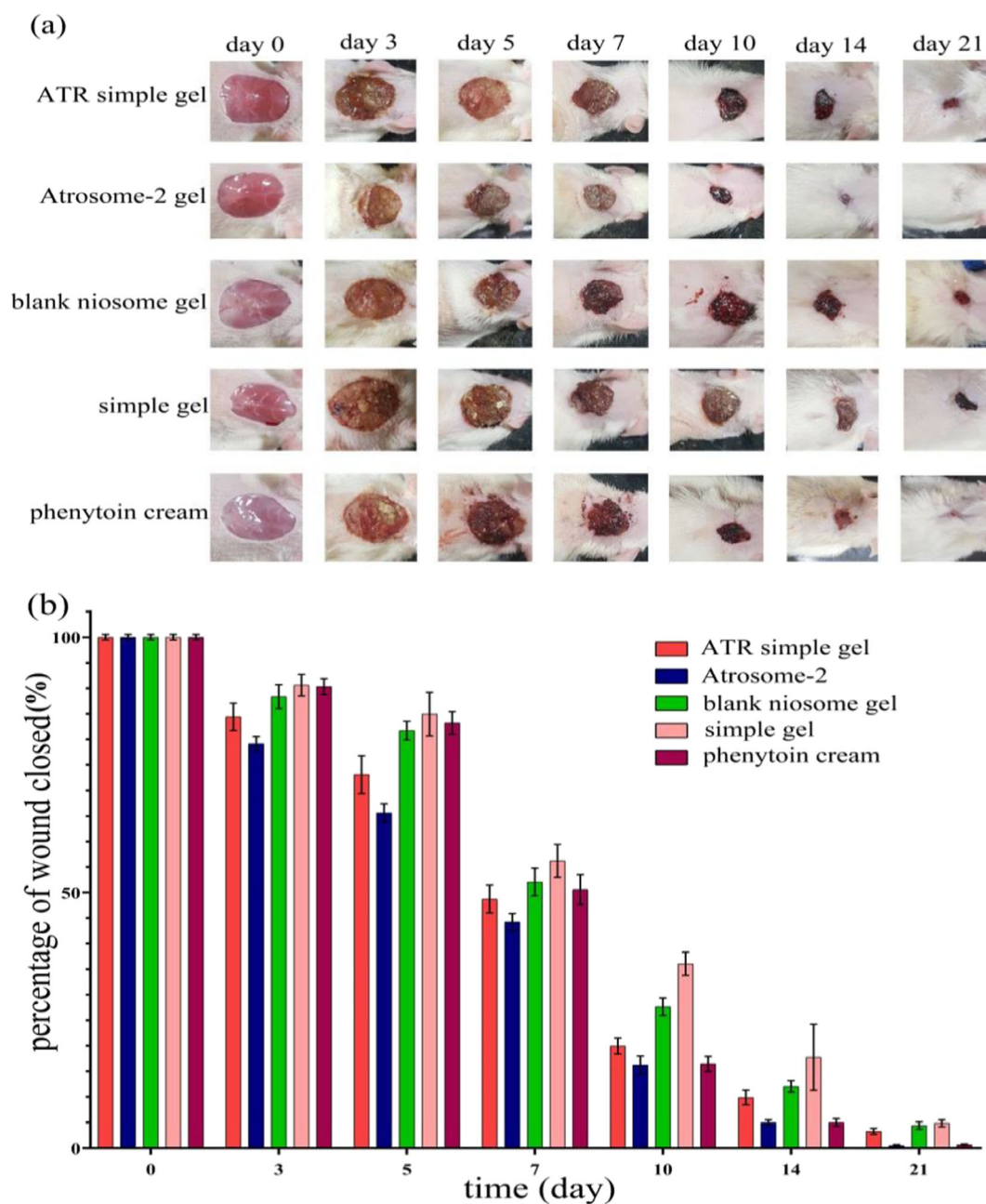


Fig. 8 Photographic representation of wound healing process in excision wound model from different experimental groups at 0, 3, 5, 7, 10, 14, and 21 days of post wounding

presented an improvement in the reepithelialization procedure while reducing the formation of inflammatory infiltrates and granulomas. The previous evidence revealed the pleiotropic impacts of statins on injuries in diabetic patients and healthy animals, although the mechanisms are not fully comprehended by these effects (43).

Lipid Peroxidation Status of Wound Tissue

The MDA levels in the tissue homogenate of cutaneous specimens were assessed to define the scope of lipid peroxidation (Figure 9a). The results of two-way ANOVA revealed that both formulation ($P < 0.001$) and time ($P < 0.001$) significantly influenced the levels of MDA. Additionally, an interaction was found between time and formulation ($P < 0.001$). Accordingly, multiple comparisons of different groups indicated lower MDA levels in Atrosome compared to the ATR simple gel (mean difference: 109.62 nmol/ μ g pr, $P < 0.001$), blank niosome gel (mean difference: 191.41 nmol/ μ g pr, $P < 0.001$), and phenytoin cream (mean difference: 53.87 nmol/ μ g pr, $P > 0.001$). It has been reported that doxorubicin niosomes reduced oxidative stress and lipid peroxidation compared with the free drug, leading to an increase in MDA levels (44).

Glutathione Peroxidase Activity in Wound Tissue

Figure 9b shows the effect of GPx activity in the skin samples of the various groups. Time ($P < 0.001$) and formulation ($P < 0.001$) significantly affected GPx levels. Furthermore, there was a relationship between formulation and time with respect to the Gpx ($P < 0.001$). Multiple comparisons of different groups revealed higher levels of GPx in the Atrosome compared to the ATR simple gel (mean difference: 0.005 nmol/ μ g pr, $P < 0.001$) and blank niosome gel (mean difference: 0.008 nmol/ μ g pr, $P < 0.001$). Meanwhile, no difference was found between the Atrosome and the phenytoin cream (mean difference: 0.0002 nmol/ μ g pr, $P = 1$). Similar findings were described by Younis et al. (45), indicating that AgNP treatment significantly increased the level of antioxidant enzymes (i.e., SOD and GPx) in comparison with silver ointment ($P < 0.001$).

Superoxide Dismutase Activity in Wound Tissue

Figure 9c shows the effect of SOD activity in the skin specimens of the various groups used in the study. The results of the two-way ANOVA revealed that both formulation ($P < 0.001$) and time ($P < 0.001$) significantly influenced the levels of SOD. Additionally, an interaction was found between time and formulation ($P < 0.001$). Accordingly, multiple comparisons of different groups indicated higher SOD levels in Atrosome compared to the ATR simple gel (mean difference: 0.32 U/ μ g protein, $P < 0.001$), blank niosome gel (mean difference: 0.45 U/ μ g protein, $P < 0.001$), and phenytoin cream (mean difference: 0.28 U/ μ g protein, $P < 0.001$).

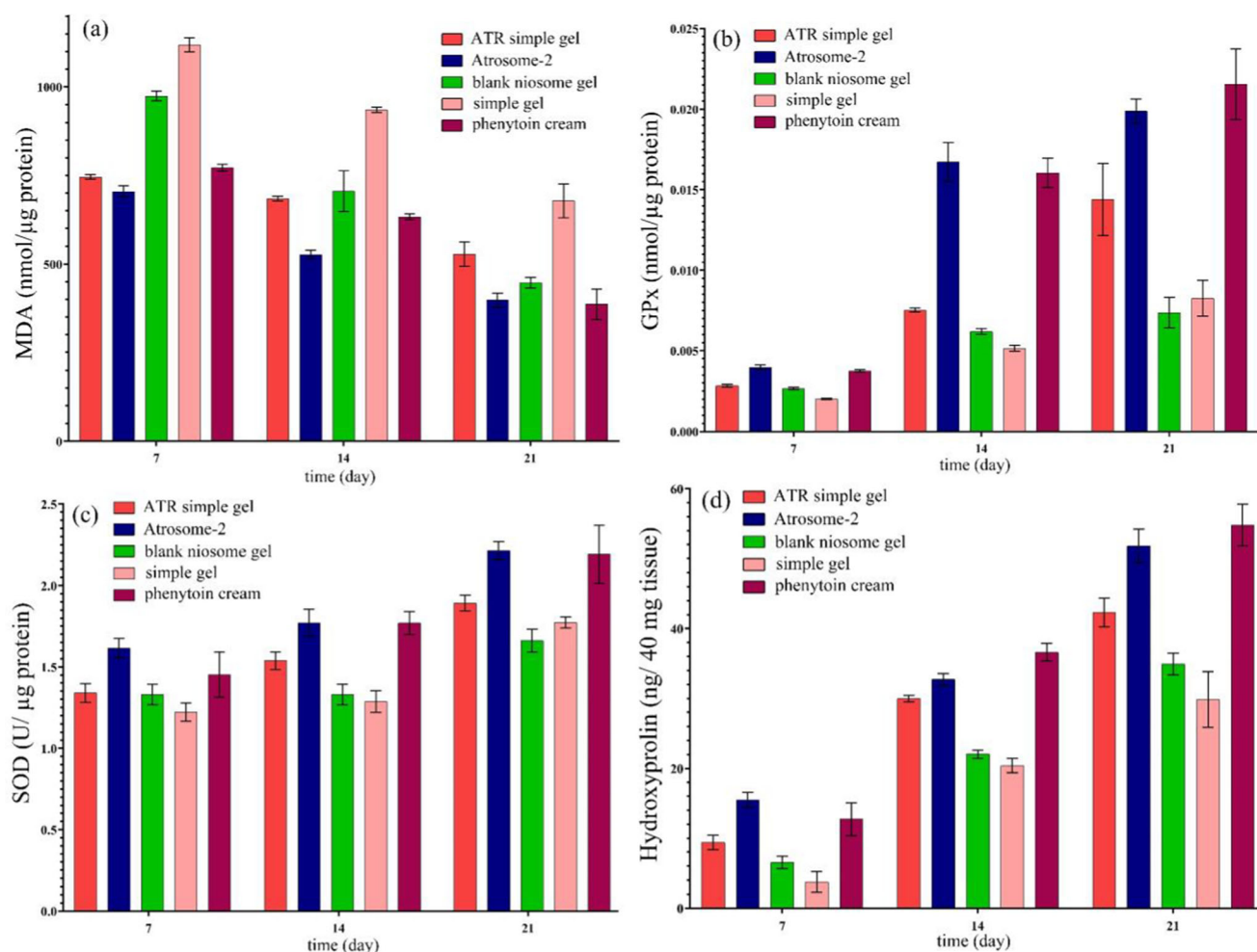


Fig. 9 Effect of ATR simple gel, Atrosome-2 gel, blank niosome gel, simple gel, and phenytoin cream on **a** MDA (lipid peroxidation product); **b** GPx; **c** SOD; and **d** hydroxyproline content and in excision wound model

0.001) and time ($P < 0.001$) significantly influenced the SOD levels. Furthermore, two-way ANOVA showed that there was an interaction between formulation and time ($P < 0.001$). Accordingly, multiple comparisons of different groups represented higher levels of SOD in the Atrosome compared to the ATR simple gel (mean difference: $0.276 \text{ U}/\mu\text{g pr}$, $P < 0.001$) and blank niosome gel (mean difference: $0.426 \text{ U}/\mu\text{g pr}$, $P < 0.001$). Likewise, no differences were observed between the Atrosome and the phenytoin cream (mean difference: $0.053 \text{ U}/\mu\text{g pr}$, $P = 0.7$). Similar findings were discovered by Farmoudeh et al. on methylene blue niosome, implying that the niosomal form of the drug caused an increase in SOD levels in comparison with methylene blue solution (15).

Hydroxyproline Production in Wound Tissue

Collagen is the principal extracellular protein in the skin tissue, and hydroxyproline is considered as the main element of collagen, making it an excellent biochemical marker for collagen content within the tissue. Therefore, the level of hydroxyproline is frequently applied as a positive marker of wound healing, since the intensification of the hydroxyproline amount can indicate any change of collagen synthesis reflecting the wound healing process in the damaged tissues (46). The hydroxyproline content in the skin specimens of groups is represented in Figure 9d. Based on the results of the two-way ANOVA, both formulation ($P < 0.001$) and time ($P < 0.001$) significantly affected the levels of hydroxyproline. Furthermore, there was an interaction between time and formulation ($P < 0.001$). Accordingly, multiple comparisons of hydroxyproline levels in the different groups showed higher levels in Atrosome compared to the ATR simple gel (mean difference: $6.77 \mu\text{g}$, $P < 0.001$) and blank niosome gel group (mean difference: $12.83 \mu\text{g}$, $P < 0.001$). There were no differences between the Atrosome and the phenytoin cream (mean difference: $0.7 \mu\text{g}$, $P = 0.9$). The results of a previous study revealed that

epithelialization, elasticity, and hydroxyproline content increased in animals treated with AgNPs compared to silver ointment owing to the strengthening effects and maturation effect of collagen fibers produced in the granulation tissue (45).

Histopathology

The histological features of the skin tissue specimens of different treatment groups on day 21 after the surgery are depicted in Figure 10. Histopathological examinations with Masson's trichrome (MT) and hematoxylin and eosin (H&E) were conducted to evaluate the mentioned criteria in histology section of the methodology section. Histological manifestations were examined. The sum of the scores in each slide was then compared across the groups using the Kruskal-Wallis test. Atrosome was better than ATR simple gel ($P < 0.05$) and blank niosome gel ($P < 0.001$). No difference was observed between the Atrosome and the phenytoin cream ($P = 0.3$). Similarly, Toker et al. have shown that the topical administration of atorvastatin increased endothelial cell regeneration and angiogenesis in the wound healing of diabetic rats (47). Additionally, the results of another study revealed that granulation tissue thickness increased in animals treated with the hydrogel matrix loaded with simvastatin microparticles compared to simvastatin (48).

CONCLUSION

The current study dealt with incorporating the atorvastatin (ATR) (a hydrophobic drug) into niosomes made by combining cholesterol and nonionic surfactants. According to solid-state investigations, ATR in the niosome was in an amorphous state, and the interaction between ATR and other excipients used in the preparation of the niosomes was ruled out. The optimized niosomal topical preparation (Atrosome-

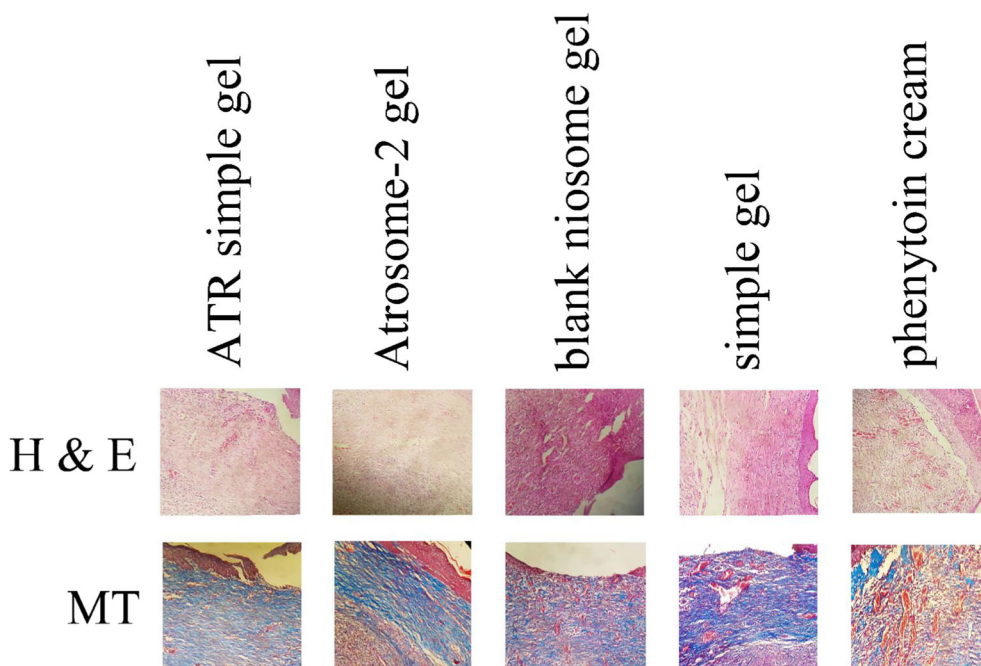


Fig. 10 Histological features of hematoxylin and eosin (H&E) and Masson's trichrome (MT) of cutaneous tissue specimen of various treatment groups on day 21 after surgery

2) presented EE%, size of the particles, the PDI, and zeta potential of 86.16 ± 0.59 %, 196 ± 6 nm, 0.46 ± 0.05 , and -20.73 ± 0.98 mV, respectively. In the MTT assay, no cytotoxicity was found for the enhanced Atrosome because of the higher percentage of cell viability (about 99%). According to macroscopic, pathological, and biochemical investigations of surgical wounds, the healing rate in the Atrosome group was greater than in other groups. Hence, the ATR niosomal gel demonstrated the maximum wound healing power with complete epithelization and wound closure within 21 days. Thus, the present study could present a novel method for effective wound healing using the topical application of an ATR niosomal gel. The current formulated niosomal form of ATR was only examined on rats, but to prove this clinically, further clinical studies are required.

AUTHOR CONTRIBUTION

Shidrokh Abootorabi: Conceptualization, Investigation, Methodology, Writing-review and editing, Writing-original draft. Jafar Akbari: Conceptualization, Supervision. Majid Saeedi: Supervision, Formal analysis, review and editing. Mohammad Seyedabadi: Methodology, Investigation. Mohammad Ranaee: Methodology, Investigation. Kofi Asare-Addo: Review and editing. Ali Nokhodchi: Writing-review and editing.

FUNDING

This project was funded by award no.7096 from the research council of Mazandaran University of Medical Sciences.

DECLARATIONS

Conflict of Interest The authors declare no competing interests.

Open Access This article is licensed under a Creative Commons Attribution 4.0 International License, which permits use, sharing, adaptation, distribution and reproduction in any medium or format, as long as you give appropriate credit to the original author(s) and the source, provide a link to the Creative Commons licence, and indicate if changes were made. The images or other third party material in this article are included in the article's Creative Commons licence, unless indicated otherwise in a credit line to the material. If material is not included in the article's Creative Commons licence and your intended use is not permitted by statutory regulation or exceeds the permitted use, you will need to obtain permission directly from the copyright holder. To view a copy of this licence, visit <http://creativecommons.org/licenses/by/4.0/>.

REFERENCES

- Ashkani-Esfahani S, Hosseinabadi OK, Moezzi P, Moafpourian Y, Kardeh S, Rafiee S, Fatheazam R, Noorafshan A, Nadimi E, Mehrvarz S, Khoshneviszadeh M, Khoshneviszadeh M. Verapamil, a calcium-channel blocker, improves the wound healing process in rats with excisional full-thickness skin wounds based on stereological parameters. *Adv Skin Wound Care*. 2016;29(8):371–4. <https://doi.org/10.1097/01.ASW.0000488666.03896.e6>.
- Cordeiro JV, Jacinto A. The role of transcription-independent damage signals in the initiation of epithelial wound healing. *Nat Rev Mol Cell Biol*. 2013;14(4):249–62. <https://doi.org/10.1038/nrm3541>.
- Koh TJ, DiPietro LA. Inflammation and wound healing: the role of the macrophage. *Expert Rev Mol Med*. 2011;13:E23. <https://doi.org/10.1017/S1462399411001943>.
- Singer AJ, Clark RA. Cutaneous wound healing. *N Engl J Med*. 1999;341(10):738–46. <https://doi.org/10.1056/NEJM199909023411006>.
- Nagase H, Woessner JF. Matrix metalloproteinases. *J Biol Chem*. 1999;274(31):21491–4. <https://doi.org/10.1074/jbc.274.31.21491>.
- Boggio RF, Freitas VM, Cassiola FM, Urabayashi M, Machado-Santelli GM. Effect of a calcium-channel blocker (verapamil) on the morphology, cytoskeleton and collagenase activity of human skin fibroblasts. *Burns*. 2011;37(4):616–25. <https://doi.org/10.1016/j.burns.2010.07.012>.
- Farsaei S, Khalili H, Farboud ES. Potential role of statins on wound healing: review of the literature. *Int Wound J*. 2012;9(3):238–47. <https://doi.org/10.1111/j.1742-481X.2011.00888.x>.
- Shahraeini SS, Akbari J, Saeedi M, Morteza-Semnani K, Abootorabi S, Dehghanpoor M, Rostamkalaei SS, Nokhodchi A. Atorvastatin solid lipid nanoparticles as a promising approach for dermal delivery and an anti-inflammatory agent. *AAPS PharmSciTech*. 2020;21(7):1–10. <https://doi.org/10.1208/s12249-020-01807-9>.
- Akbari J, Saeedi M, Enayatifard R, Morteza-Semnani K, Hashemi SMH, Babaei A, et al. Curcumin Niosomes (curcusesomes) as an alternative to conventional vehicles: a potential for efficient dermal delivery. *J Drug Deliv Sci Technol*. 2020;60:102035. <https://doi.org/10.1016/j.jddst.2020.102035>.
- National Center for Biotechnology Information (2021). PubChem Compound Summary for CID 60823, Atorvastatin. Retrieved July 14, 2021 from <https://pubchem.ncbi.nlm.nih.gov/compound/Atorvastatin>.
- Goffin V, Henry F, Piérard-Franchimont C, Piérard GE. Penetration enhancers assessed by corneoxenometry. *Skin Pharmacol Physiol*. 2000;13(5):280–4. <https://doi.org/10.1159/000029934>.
- Khatoun M, Shah KU, Din FU, Shah SU, Rehman AU, Dilawar N, Khan AN. Proniosomes derived niosomes: recent advancements in drug delivery and targeting. *Drug Deliv*. 2017;24(2):56–69. <https://doi.org/10.1080/10717544.2017.1384520>.
- Marianecchi C, Di Marzio L, Rinaldi F, Celia C, Paolino D, Alhaique F, et al. Niosomes from 80s to present: the state of the art. *Adv Colloid Interf Sci*. 2014;205:187–206. <https://doi.org/10.1016/j.cis.2013.11.018>.
- Aghajani A, Kazemi T, Enayatifard R, Amiri FT, Narenji M. Investigating the skin penetration and wound healing properties of niosomal pentoxifylline cream. *Eur J Pharm Sci*. 2020;151:105434. <https://doi.org/10.1016/j.ejps.2020.105434>.
- Farmoudeh A, Akbari J, Saeedi M, Ghasemi M, Asemi N, Nokhodchi A. Methylene blue-loaded niosome: preparation, physicochemical characterization, and in vivo wound healing assessment. *Drug Deliv Transl Res*. 2020;10(5):1428–41. <https://doi.org/10.1007/s13346-020-00715-6>.
- El-Ridy MS, Yehia SA, Elsayed I, Younis MM, Abdel-Rahman RF, El-Gamil MA. Metformin hydrochloride and wound healing: from nanoformulation to pharmacological evaluation. *J Liposome Res*. 2019;29(4):343–56. <https://doi.org/10.1080/08982104.2018.1556291>.
- Radmard A, Saeedi M, Morteza-Semnani K, Hashemi SMH, Nokhodchi A. An eco-friendly and green formulation in lipid nanotechnology for delivery of a hydrophilic agent to the skin in the treatment and management of hyperpigmentation complaints: Arbutin niosome (Arbusome). *Colloids Surf B: Biointerfaces*. 2021;201:111616. <https://doi.org/10.1016/j.colsurfb.2021.111616>.
- Delmas T, Couffin A-C, Bayle PA, De Crecy F, Neumann E, Vinet F, et al. Preparation and characterization of highly stable

- lipid nanoparticles with amorphous core of tuneable viscosity. *J Colloid Interface Sci.* 2011;360(2):471–81. <https://doi.org/10.1016/j.jcis.2011.04.080>.
19. Sharma M, Gupta N, Gupta S. Implications of designing clarithromycin loaded solid lipid nanoparticles on their pharmacokinetics, antibacterial activity and safety. *RSC Adv.* 2016;6(80):76621–31. <https://doi.org/10.1039/C6RA12841F>.
 20. Boskabadi M, Saeedi M, Akbari J, Morteza-Semnani K, Hashemi SMH, Babaei A. Topical gel of vitamin A solid lipid nanoparticles: A hopeful promise as a dermal delivery system. *Adv Pharm Bull.* 2021;11(4):663–74. doi: 10.34172/apb.2021.075.
 21. Guo D, Dou D, Li X, Zhang Q, Bhutto ZA, Wang L. Ivermectin-loaded solid lipid nanoparticles: preparation, characterisation, stability and transdermal behaviour. *Artif Cells Nanomed Biotechnol.* 2018;46(2):255–62. <https://doi.org/10.1080/21691401.2017.1307207>.
 22. Kalhapure RS, Mocktar C, Sikwal DR, Sonawane SJ, Kathiravan MK, Skelton A, Govender T. Ion pairing with linoleic acid simultaneously enhances encapsulation efficiency and antibacterial activity of vancomycin in solid lipid nanoparticles. *Colloids Surf B: Biointerfaces.* 2014;117:303–11. <https://doi.org/10.1016/j.colsurfb.2014.02.045>.
 23. Shaw J, Hughes C, Lagan K, Bell P. The clinical effect of topical phenytoin on wound healing: a systematic review. *Br J Dermatol.* 2007;157(5):997–1004. <https://doi.org/10.1111/j.1365-2133.2007.08160.x>.
 24. PENDSE AK, SHARMA A, SODANI A, HADA S. Topical phenytoin in wound healing. *Int J Dermatol.* 1993;32(3):214–7. <https://doi.org/10.1111/j.1365-4362.1993.tb02799.x>.
 25. Asai J, Takenaka H, Hirakawa S, Sakabe J-i, Hagura A, Kishimoto S, et al. Topical simvastatin accelerates wound healing in diabetes by enhancing angiogenesis and lymphangiogenesis. *Am J Pathol.* 2012;181(6):2217–24. <https://doi.org/10.1016/j.ajpath.2012.08.023>.
 26. Uchiyama M, Mihara M. Determination of malonaldehyde precursor in tissues by thiobarbituric acid test. *Anal Biochem.* 1978;86(1):271–8. [https://doi.org/10.1016/0003-2697\(78\)90342-1](https://doi.org/10.1016/0003-2697(78)90342-1).
 27. Biasibetti H, Pierozan H, Rodrigues AF, Manfredini V, Wyse AT. Hypoxanthine intrastratial administration alters neuroinflammatory profile and redox status in striatum of infant and young adult rats. *Mol Neurobiol.* 2017;54(4):2790–800. <https://doi.org/10.1007/s12035-016-9866-6>.
 28. Wihastyoko HY, Soeharto S, Widjajanto E, Handono K, Pardjianto B. Effect of papain enzyme administration in pH alteration, VEGF phosphorylation, and its impact on collagen degradation using a rat model of abnormal scarring. *Trop J Pharm Res.* 2021;20(5):1022–17. <https://doi.org/10.4314/tjpr.v20i5.19>.
 29. Muhammad AA, Arulselvan P, Cheah PS, Abas F, Fakurazi S. Evaluation of wound healing properties of bioactive aqueous fraction from *Moringa oleifera* Lam on experimentally induced diabetic animal model. *Drug Des Devel.* 2016;10:1715–30. <https://doi.org/10.2147/DDDT.S96968>.
 30. Silva LAB, Novaes AB Jr, de Oliveira RR, Nelson-Filho P, Santamaria M Jr, Silva RAB. Antimicrobial photodynamic therapy for the treatment of teeth with apical periodontitis: a histopathological evaluation. *J Endod.* 2012;38(3):360–6. <https://doi.org/10.1016/j.joen.2011.12.023>.
 31. Tajbakhsh M, Saeedi M, Morteza-Semnani K, Akbari J, Nokhodchi A. Innovation of testosome as a green formulation for the transdermal delivery of testosterone enanthate. *J Drug Deliv Sci Technol.* 2020;57:101685. <https://doi.org/10.1016/j.jddst.2020.101685>.
 32. Nasser B. Effect of cholesterol and temperature on the elastic properties of niosomal membranes. *Int J Pharm.* 2005;300(1–2):95–101. <https://doi.org/10.1016/j.ijpharm.2005.05.009>.
 33. Mokhtar M, Sammour OA, Hammad MA, Megrab NA. Effect of some formulation parameters on flurbiprofen encapsulation and release rates of niosomes prepared from proniosomes. *Int J Pharm.* 2008;361(1–2):104–11. <https://doi.org/10.1016/j.ijpharm.2008.05.031>.
 34. Mishra V, Bansal KK, Verma A, Yadav N, Thakur S, Sudhakar K, Rosenholm J. Solid lipid nanoparticles: Emerging colloidal nano drug delivery systems. *Pharmaceutics.* 2018;10(4):191. <https://doi.org/10.3390/pharmaceutics10040191>.
 35. Akbari J, Saeedi M, Morteza-Semnani K, Rostamkalaei SS, Asadi M, Asare-Addo K, Nokhodchi A. The design of naproxen solid lipid nanoparticles to target skin layers. *Colloids Surf B: Biointerfaces.* 2016;145:626–33. <https://doi.org/10.1016/j.colsurfb.2016.05.064>.
 36. Taymouri S, Varshosaz J. Effect of different types of surfactants on the physical properties and stability of carvedilol naniosomes. *Adv Biomed Res.* 2016;5. <https://doi.org/10.4103/2277-9175.178781>.
 37. Siepmann J, Siepmann F. Mathematical modeling of drug delivery. *Int J Pharm.* 2008;364(2):328–43. <https://doi.org/10.1016/j.ijpharm.2008.09.004>.
 38. Bhattacharjee S. DLS and zeta potential—what they are and what they are not? *J Control Release.* 2016;235:337–51. <https://doi.org/10.1016/j.jconrel.2016.06.017>.
 39. Brydson R, Brown A, Hodges C, Abellan P, Hondon N. Microscopy of nanoparticulate dispersions. *J Microsc.* 2015;260(3):238–47. <https://doi.org/10.1111/jmi.12290>.
 40. Elmowafy M, Ibrahim HM, Ahmed MA, Shalaby K, Salama A, Hefesha H. Atorvastatin-loaded nanostructured lipid carriers (NLCs): strategy to overcome oral delivery drawbacks. *Drug Deliv.* 2017;24(1):932–41. <https://doi.org/10.1080/10717544.2017.1337823>.
 41. Çelik H, Karahan H, Kelicen-Uğur P. Effect of atorvastatin on $\text{A}\beta_{1-42}$ -induced alteration of SESN2, SIRT1, LC3II and TPP1 protein expressions in neuronal cell cultures. *J Pharm Pharmacol.* 2020;72(3):424–36. <https://doi.org/10.1111/jphp.13208>.
 42. Morsy MA, Abdel-Latif RG, Nair AB, Venugopala KN, Ahmed AF, Elsewedy HS, Shehata TM. Preparation and evaluation of atorvastatin-loaded nanoemulgel on wound-healing efficacy. *Pharmaceutics.* 2019;11(11):609. <https://doi.org/10.3390/pharmaceutics11110609>.
 43. Adami M, da Silveira PA, Mendes DAGB, da Silva Horinouchi CD, Cabrini DA, Otuki MF. Simvastatin ointment, a new treatment for skin inflammatory conditions. *J Dermatol Sci.* 2012;66(2):127–35. <https://doi.org/10.1016/j.jdermsci.2012.02.015>.
 44. Pawar S, Shevalkar G, Vavia P. Glucosamine-anchored doxorubicin-loaded targeted nano-niosomes: pharmacokinetic, toxicity and pharmacodynamic evaluation. *J Drug Target.* 2016;24(8):730–43. <https://doi.org/10.3109/1061186X.2016.1154560>.
 45. Younis N, El Semary N, Mohamed M. Silver nanoparticles green synthesis via cyanobacterium *Phormidium* sp.: characterization, wound healing, antioxidant, antibacterial, and anti-inflammatory activities. *Eur Rev Med Pharmacol Sci.* 2021;25(7):3083–96. https://doi.org/10.26355/eurrev_202104_25563.
 46. Hajji S, Khedir SB, Hamza-Mnif I, Hamdi M, Jedidi I, Kallel R, Boufi S, Nasri M. Biomedical potential of chitosan-silver nanoparticles with special reference to antioxidant, antibacterial, hemolytic and in vivo cutaneous wound healing effects. *BAA General Subjects.* 2019;1863(1):241–54. <https://doi.org/10.1016/j.bbagen.2018.10.010>.
 47. Toker S, Gulcan E, Cayci MK, Olgun EG, Erbilin E, Özyay Y. Topical atorvastatin in the treatment of diabetic wounds. *Am J Med Sci.* 2009;338(3):201–4. <https://doi.org/10.1097/MAJ.0b013e3181aaf209>.
 48. Yasasvini S, Anusa R, VedhaHari B, Prabhu P, RamyaDevi D. Topical hydrogel matrix loaded with Simvastatin microparticles for enhanced wound healing activity. *Mater Sci Eng C.* 2017;72:160–7. <https://doi.org/10.1016/j.msec.2016.11.038>.